Electronic Supplementary Information (ESI) for *Dalton Transactions*

Synthesis, crystal structures and magnetic properties of a series of chair-like heterometallic [Fe_4Ln_2] (Ln = Gd^{III}, Dy^{III}, Ho^{III}, Er^{III}) complexes with mixed organic ligands

Hui-Sheng Wang,*[,a] Qiao-Qiao Long,[a] Zhao-Bo Hu,[b] Lin Yue,[a] Feng-Jun Yang,[a] Cheng-Ling Yin,[a] Zhi-Quan Pan,[a] Yi-Quan Zhang,*[c] and You Song*[,b]

[a] School of Chemistry and Environmental Engineering, Wuhan Institute of Technology, Key Laboratory for Green Chemical Process of Ministry of Education, Wuhan 430074, P. R. China
[b] State Key Laboratory of Coordinate Chemistry, Nanjing National Laboratory of Microstructures, School of Chemistry and Chemical Engineering, Nanjing University, Nanjing 210023, P. R. China
[c] Jiangsu Key Laboratory for NSLSCS, School of Physical Science and Technology, Nanjing Normal University, Nanjing 210023, China

Email: wangch198201@163.com (H.-S.Wang), yousong@nju.edu.cn (Y. S.), zhangyiquan@njnu.edu.cn (Y.-Q.Zhang)

Table S1. Crystallographic data for complexes **1-4**.

Compounds	**1**	**2**	**3**	**4**
Formula	$C_{60}H_{53}Cl_4Fe_4Gd_2N_{13}O_{20}$	$C_{60}H_{55}Cl_4Dy_2Fe_4N_{13}O_{21}$	$C_{58}H_{54}Cl_4Fe_4Ho_2N_{12}O_{22}$	$C_{60}H_{59}Cl_4Er_2Fe_4N_{13}O_{23}$
Formula weight	1955.85	1984.37	1966.19	2029.92
Temperature	173(2) K	173(2) K	173(2) K	173(2) K
Crystal color	yellow	yellow	yellow	yellow
Crystal size (mm)	0.36 × 0.18 × 0.17	0.38 × 0.34 × 0.31	0.34 × 0.33 × 0.21	0.35 × 0.21 × 0.18
Crystal system	triclinic	triclinic	triclinic	triclinic
Space group	$P\,\bar{1}$	$P\,\bar{1}$	$P\,\bar{1}$	$P\,\bar{1}$
a (Å)	13.9064(5)	13.9055(6)	13.8523(5)	13.8617(7)
b (Å)	15.7148(5)	15.7120(7)	15.6979(6)	15.6909(8)
c (Å)	20.7911(8)	20.7958(10)	20.7364(9)	20.7168(9)
α (°)	81.3690(10)	81.299(2)	81.4060(10)	81.361(2)
β (°)	83.2030(10)	83.309(2)	83.0750(10)	83.042(2)
γ (°)	66.0340(10)	65.9440(10)	66.2000(10)	66.101(2)
V(Å^3)	4096.6(3)	4093.6(3)	4070.3(3)	4063.8(3)
Z	2	2	2	2
D_c (g/cm^{-3})	1.586	1.610	1.604	1.659
μ(Mo Kα) (mm^{-1})	2.485	2.694	2.817	2.943
F(000)	1928	1956	1936	2004
θ range (°)	2.86~25.38	2.86~25.37	2.80~25.40	2.75~25.41
Index ranges	$-16 \leq h \leq 16$ $-18 \leq k \leq 16$ $-24 \leq l \leq 24$	$-16 \leq h \leq 16$ $-18 \leq k \leq 18$ $-24 \leq l \leq 24$	$-16 \leq h \leq 16$ $-18 \leq k \leq 18$ $-24 \leq l \leq 24$	$-16 \leq h \leq 16$ $-18 \leq k \leq 18$ $-23 \leq l \leq 24$
Reflections collected	31896	46802	47139	36264
Restraints/parameters	3/922	3/932	0/919	7/956
Unique reflections [R_{int}]	14323 [0.0572]	14388 [0.0380]	14300 [0.0313]	14022 [0.0647]
Reflections with $I > 2\sigma(I)$	10248	11684	11736	10024
Goodness-of-fit on F^2	1.088	1.047	1.057	1.032
Final R indices [I>2σ(I)]	$R_1{}^a = 0.0390$, $wR_2{}^b = 0.0597$	$R_1{}^a = 0.0331$, $wR_2{}^b = 0.0729$	$R_1{}^a = 0.0295$, $wR_2{}^b = 0.0670$	$R_1{}^a = 0.0418$, $wR_2{}^b = 0.0811$
Final R indices (all data)	$R_1{}^a = 0.0698$, $wR_2{}^b = 0.0632$	$R_1{}^a = 0.0486$, $wR_2{}^b = 0.0771$	$R_1{}^a = 0.0434$, $wR_2{}^b = 0.0715$	$R_1{}^a = 0.0741$, $wR_2{}^b = 0.0874$
S (all data)	1.089	1.049	1.057	1.033
$(\Delta\rho)_{max,min}$/e Å^{-3}	0.962 and -0.844	2.377 and -1.440	1.707 and -1.312	1.694 and -1.543

$^aR_1 = \Sigma(||F_o| - |F_c||)/\Sigma|F_o|$. ^{b} $wR_2 = [\Sigma[w(F_o{}^2 - F_c{}^2)^2]/\Sigma[w(F_o{}^2)^2]]^{1/2}$, $w = 1/[\sigma^2(F_o{}^2) + [(ap)^2 + bp]$, where $p = [\max(F_o{}^2, 0) + 2F_c{}^2]/3$.

Table S2. Selected bond lengths (Å) and angles (°) for **1**.

Bond lengths			
Fe(1)-O(3)	1.947(3)	Fe(2)-Cl(2)	2.297(14)
Fe(1)-O(5)	1.964(3)	Gd(1)-O(1)	2.601(3)
Fe(1)-O(1)	2.038(3)	Gd(1)-O(2)	2.388(3)
Fe(1)-N(1)	2.178(4)	Gd(1)-O(4)	2.390(3)
Fe(1)-N(3)	2.182(4)	Gd(1)-O(5)	2.345(3)
Fe(1)-Cl(1)	2.333(13)	Gd(1)-O(6)	2.459(3)
Fe(2)-O(2)	1.950(3)	Gd(1)-O(7)	2.540(3)
Fe(2)-O(6)	1.972(3)	Gd(1)-O(8)	2.497(4)
Fe(2)-O(4)	2.043(3)	Gd(1)-O(10)	2.357(3)
Fe(2)-N(4)	2.140(4)	Gd(1)-N(5)	2.454(4)
Fe(2)-N(2)	2.202(4)		
Bond angles			
O(3)-Fe(1)-O(5)	96.20(13)	N(4)-Fe(2)-Cl(2)	93.45(11)
O(3)-Fe(1)-O(1)	94.61(12)	N(2)-Fe(2)-Cl(2)	96.45(10)
O(5)-Fe(1)-O(1)	82.81(12)	O(6)-Gd(1)-N(6)	99.15(13)
O(3)-Fe(1)-N(1)	165.17(13)	O(5)-Gd(1)-O(8)	121.96(12)
O(5)-Fe(1)-N(1)	94.94(15)	O(10)-Gd(1)-O(8)	75.74(14)
O(1)-Fe(1)-N(1)	77.09(13)	O(4)-Gd(1)-O(8)	92.61(12)
N(4)-Fe(2)-N(2)	88.86(15)	O(5)-Gd(1)-N(6)	96.42(13)
O(2)-Fe(2)-Cl(2)	103.73(10)	O(10)-Gd(1)-N(6)	70.54(13)
O(6)-Fe(2)-Cl(2)	98.87(10)	O(4)-Gd(1)-N(6)	116.76(13)
O(4)-Fe(2)-Cl(2)	169.80(10)	O(2)-Gd(1)-N(6)	159.94(13)

Table S3. Selected bond lengths (Å) and angles (°) for **2**.

Bond lengths			
Fe(1)-O(3)	1.942(3)	Fe(2)-Cl(2)	2.230(12)
Fe(1)-O(5)	1.956(3)	Dy(1)-O(5)	2.342(3)
Fe(1)-O(1)	2.028(3)	Dy(1)-O(10)	2.352(3)
Fe(1)-N(1)	2.194(4)	Dy(1)-O(2)	2.399(3)
Fe(1)-N(3)	2.199(4)	Dy(1)-O(4)	2.400(3)
Fe(1)-Cl(1)	2.341(12)	Dy(1)-O(6)	2.434(3)
Fe(2)-O(2)	1.958(3)	Dy(1)-N(5)	2.443(3)
Fe(2)-O(6)	1.966(3)	Dy(1)-O(8)	2.481(3)
Fe(2)-O(4)	2.043(3)	Dy(1)-O(7)	2.541(3)
Fe(2)-N(4)	2.138(3)	Dy(1)-O(1)	2.638(3)
Fe(2)-N(2)	2.138(3)		
Bond angles			
O(5)-Dy(1)-O(10)	88.96(10)	O(5)-Fe(1)-N(3)	171.34(13)
O(5)-Dy(1)-O(2)	84.79(10)	O(2)-Fe(2)-O(6)	83.47(12)
O(10)-Dy(1)-O(2)	127.04(10)	O(2)-Fe(2)-O(4)	87.48(11)
O(5)-Dy(1)-O(4)	144.13(10)	O(6)-Fe(2)-O(4)	80.11(11)
O(10)-Dy(1)-O(4)	86.07(10)	O(2)-Fe(2)-N(4)	157.47(12)

O(2)-Dy(1)-O(4)	70.42(9)	O(3)-Fe(1)-N(3)	77.33(13)
O(3)-Fe(1)-O(5)	95.70(12)	O(6)-Fe(2)-N(4)	109.24(13)
O(3)-Fe(1)-O(1)	92.85(11)	O(4)-Fe(2)-N(4)	76.91(12)
O(5)-Fe(1)-O(1)	83.63(11)	O(2)-Fe(2)-N(2)	75.71(12)

Table S4. Selected bond lengths (Å) and angles (°) for **3**.

Bond lengths			
Fe(1)-O(1)	1.960(3)	Fe(2)-Cl(2)	2.340(12)
Fe(1)-O(5)	1.963(3)	Ho(1)-O(10)	2.318(3)
Fe(1)-O(4)	2.044(2)	Ho(1)-O(6)	2.318(3)
Fe(1)-N(4)	2.126(3)	Ho(1)-O(1)	2.355(3)
Fe(1)-N(1)	2.214(3)	Ho(1)-O(4)	2.372(2)
Fe(1)-Cl(1)	2.295(12)	Ho(1)-O(5)	2.409(3)
Fe(2)-O(3)	1.942(3)	Ho(1)-N(5)	2.411(3)
Fe(2)-O(6)	1.961(3)	Ho(1)-O(8)	2.436(3)
Fe(2)-O(2)	2.024(3)	Ho(1)-O(7)	2.525(3)
Fe(2)-N(2)	2.193(3)	Ho(1)-O(2)	2.617(3)
Fe(2)-N(3)	2.197(3)		
Bond angles			
O(1)-Fe(1)-O(5)	83.35(11)	O(6)-Fe(2)-N(2)	95.10(12)
O(1)-Fe(1)-O(4)	86.46(10)	O(2)-Fe(2)-N(2)	77.11(11)
O(5)-Fe(1)-O(4)	79.71(10)	O(10)-Ho(1)-O(6)	88.57(9)
O(5)-Fe(1)-N(4)	109.00(11)	O(1)-Ho(1)-O(4)	70.96(8)
O(4)-Fe(1)-N(4)	77.52(11)	O(6)-Ho(1)-O(1)	85.55(9)
O(1)-Fe(1)-N(1)	75.90(11)	O(10)-Ho(1)-O(4)	85.47(9)
O(3)-Fe(2)-O(6)	95.33(11)	O(1)-Ho(1)-O(5)	66.40(9)
O(3)-Fe(2)-O(2)	93.12(10)	O(4)-Ho(1)-O(5)	65.00(8)
O(6)-Fe(2)-O(2)	83.10(11)	O(1)-Ho(1)-N(5)	80.72(10)
O(3)-Fe(2)-N(2)	164.73(12)	O(4)-Ho(1)-N(5)	130.41(10)

Table S5. Selected bond lengths (Å) and angles (°) for **4**.

Bond lengths			
Fe(1)-O(5)	1.957(4)	Fe(2)-Cl(2)	2.289(17)
Fe(1)-O(1)	1.955(4)	Er(1)-O(6)	2.298(4)
Fe(1)-O(3)	2.042(4)	Er(1)-O(10)	2.311(4)
Fe(1)-N(3)	2.132(5)	Er(1)-O(1)	2.337(4)
Fe(1)-N(1)	2.197(5)	Er(1)-O(3	2.352(4)
Fe(1)-Cl(1)	2.344(17)	Er(1)-N(5)	2.398(5)
Fe(2)-O(4)	1.935(4)	Er(1)-O(5)	2.414(4)
Fe(2)-O(6)	1.961(4)	Er(1)-O(7)	2.424(4)
Fe(2)-O(2)	2.037(4)	Er(1)-O(8)	2.523(4)
Fe(2)-N(2)	2.170(5)	Er(1)-O(2)	2.570(4)
Fe(2)-N(4)	2.169(5)		
Bond angles			

O(6)-Er(1)-O(10)	88.71(14)	O(5)-Fe(1)-O(3)	79.81(16)
O(6)-Er(1)-O(1)	85.40(13)	O(1)-Fe(1)-N(3)	157.66(19)
O(10)-Er(1)-O(1)	130.01(13)	O(5)-Fe(1)-N(3)	106.98(18)
O(6)-Er(1)-O(3)	143.61(13)	O(1)-Fe(1)-O(5)	83.94(16)
O(10)-Er(1)-O(3)	86.36(13)	O(4)-Fe(2)-O(2)	94.38(15)
O(1)-Er(1)-O(3)	70.76(13)	O(4)-Fe(2)-O(6)	96.98(16)
O(6)-Er(1)-N(5)	68.08(15)	O(4)-Fe(2)-N(2)	165.26(18)
O(10)-Er(1)-N(5)	142.25(14)	O(6)-Fe(2)-N(2)	94.73(18)
O(1)-Er(1)-N(5)	79.20(15)	N(2)-Fe(2)-N(4)	90.92(19)
O(1)-Fe(1)-O(3)	85.55(16)	O(2)-Fe(2)-N(4)	92.11(17)

Table S6. Bond Valence Sum (BVS)[a,b] Calculations for Fe and Selected Oxygen atoms in **2**.

Atom	Fe^{II}	Fe^{III}	
Fe1	2.732	2.980	
Fe2	2.780	3.035	
	BVS	Assignment	Group
O1	1.597	RO^{-} (μ_2)	$(py)_2CO_2^{2-}$
O2	1.910	RO^{-} (μ_2)	$(py)_2CO_2^{2-}$
O3	1.599	RO^{-} (μ)	$(py)_2CO_2^{2-}$
O4	1.794	RO^{-} (μ_2)	$(py)_2CO_2^{2-}$
O5	1.909	RO^{-} (μ_2)	pdm^{2-}
O6	1.833	RO^{-} (μ_2)	pdm^{2-}
O10	0.387	H_2O	

[a] The underlined value is the one closest to the charge for which it was calculated. The oxidation state is the nearest whole number to the underlined value. [b] An O BVS in the ~1.8-2.0~1.0-1.2, and ~0.2-0.4 ranges are indicative of non-, single- and double-protonation, respectively.

Table S7. The possible geometries of nona-coordination metal centers.

Geometry	Point group	Polyhedron
EP-9	D_{9h}	Enneagon
OPY-9	C_{8v}	Octagonal pyramid
HBPY-9	D_{7h}	Heptagonal bipyramid
JTC-9	C_{3v}	Triangular cupola (J3) = trivacant cuboctahedron
JCCU-9	C_{4v}	Capped cube (Elongated square pyramid, J8)
6CCU-9	C_{4v}	Capped cube
JCSAPR-9	C_{4v}	Capped sq. antiprism (Gyroelongated square pyramid J10)
CSAPR-9	C_{4v}	Capped square antiprism
JTCTPR-9	D_{3h}	Tricapped trigonal prism (J51)
TCTPR-9	D_{3h}	Tricapped trigonal prism
JTDIC-9	C_{3v}	Tridiminished icosahedron (J63)
HH-9	C_{2v}	Hula-hoop
MFF-9	C_s	Muffin

Table S8. Deviation parameters calculated by SHAPE from each ideal polyhedron for complexes **1-4**.

Coordination geometry	**1**	**2**	**3**	**4**
	Gd1	Dy1	Ho1	Er1
EP-9	32.938	33.108	32.887	32.975
OPY-9	21.166	21.138	21.061	21.132
HBPY-9	15.395	15.409	15.409	15.471
JTC-9	14.612	14.488	14.226	14.173
JCCU-9	9.479	8.880	8.639	8.633
CCU-9	8.013	7.362	7.175	7.174
JCSAPR-9	2.963	3.039	2.926	2.821
CSAPR-9	2.297	2.430	2.349	2.294
JTCTPR-9	3.360	3.354	3.080	2.981
TCTPR-9	3.091	3.104	2.961	2.905
JTDIC-9	11.874	11.565	11.616	11.629
HH-9	10.150	9.646	9.498	9.477
MFF-9	1.644	1.755	1.701	1.682

Table S9. Best fit parameters obtained for the extended Debye model with ac susceptibility data from SQUID magnetometer of compound **2** in the applied field of 2000 Oe.

T (K)	χ_S	χ_T	τ (s)	α
1.8	0.76702	3.88962	0.00232	0.35821
2.0	0.81882	3.69341	0.00156	0.33037
2.2	0.86418	3.53713	0.00114	0.30603
2.4	0.90782	3.33515	7.55×10^{-4}	0.26823
2.6	0.95399	3.16500	5.13×10^{-4}	0.22585
2.8	0.98335	3.00455	3.30×10^{-4}	0.17793
3.0	1.00807	2.85748	2.02×10^{-4}	0.13029
3.2	1.05332	2.72938	1.22×10^{-4}	0.09545

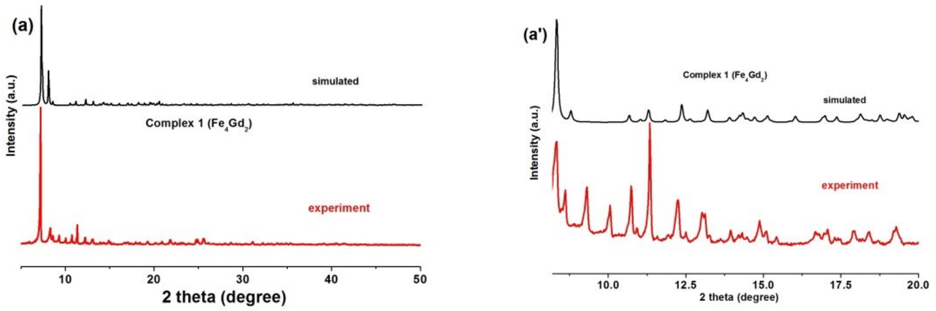

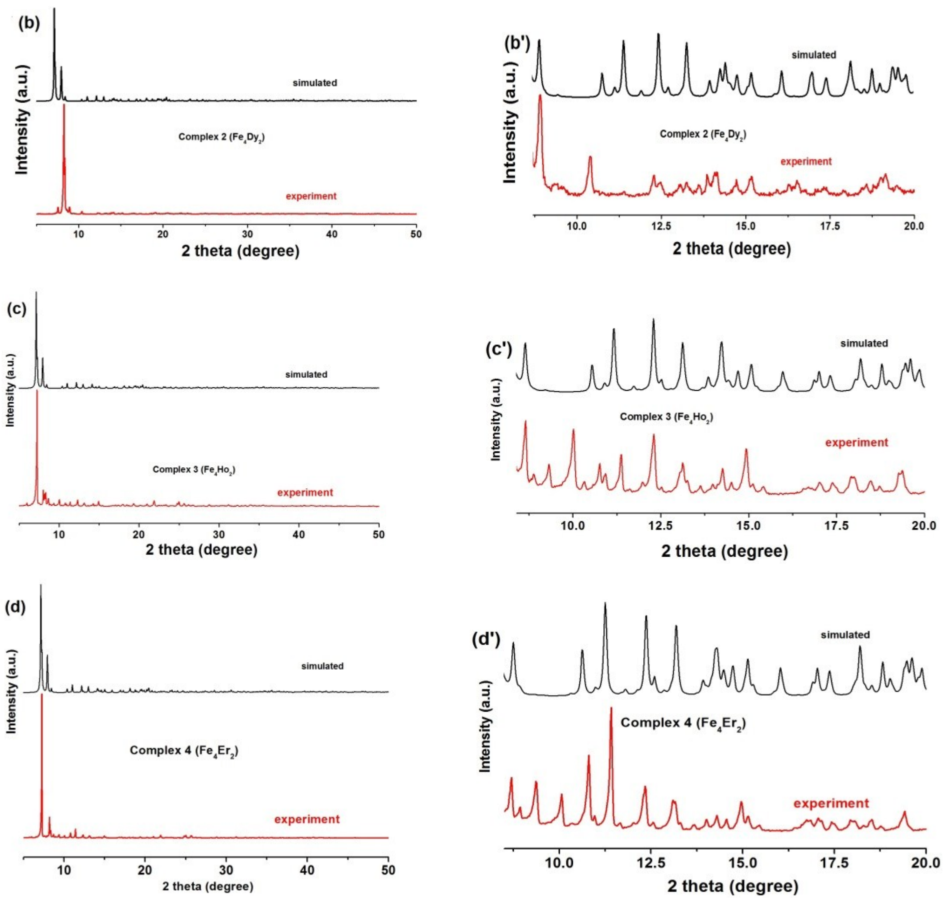

Figure S1. Plots (a)-(d) (left) show the PXRD patterns and the simulated patterns generated from single crystal diffraction data for compounds **1-4** with the 2 theta values in the range of 5-50°. To just easily, plots (a')-(d') (right) show the enlarged regions of plots (a)-(d) with the 2 theta values ranging from about 8 to 20°.

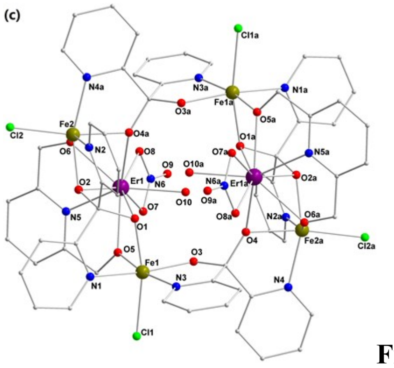

Figure S2. Molecular structures of **1**(a), **3**(b), **4**(c). For clarity, the H atoms and the non-coordinated solvent molecules are omitted (symmetry code: a: -x, 1-y, 1-z), Gd^{III} pink, Fe^{III} dark yellow, Ho^{III} light orange, Er^{III} violet, N blue, O red, Cl bright green, C gray.

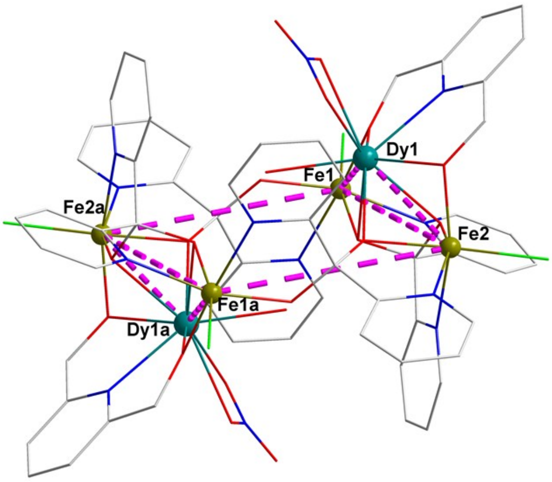

Figure S3. The chair-like core of **2**.

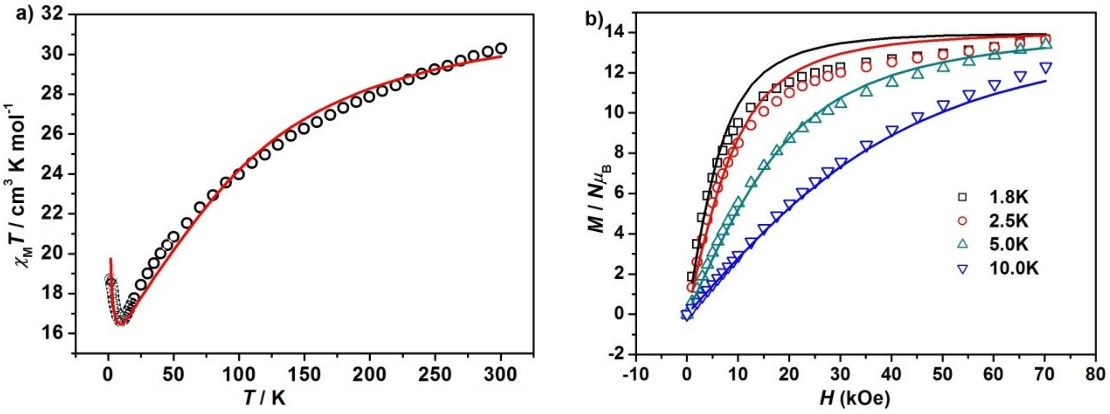

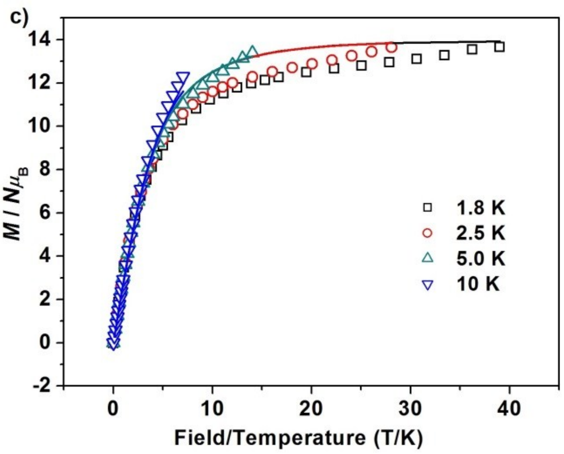

Figure S4. The plots of $\chi_{\mathrm{M}}T$ vs. *T* (a), *M* vs. *H* (b) and *M* vs. *H/T* (c) for **1**, the solid lines represent the fitted results by PHI program when the zero-field splitting parameters (*D*) were not considered.

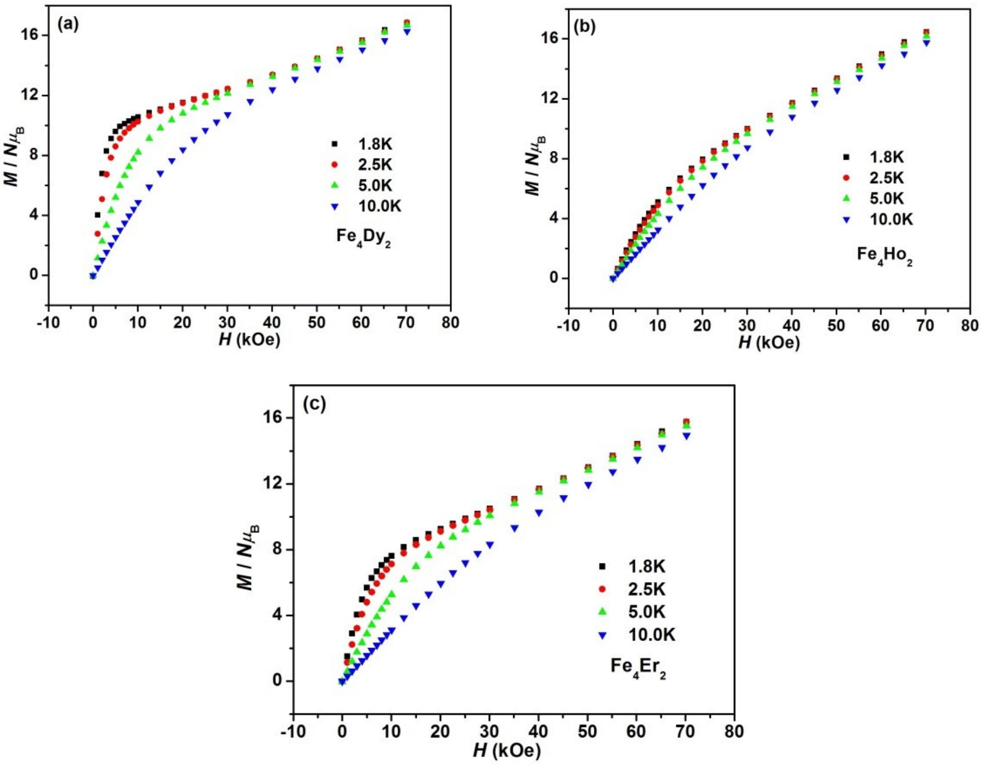

Figure S5. Magnetization *versus* field data for complexes **2**(a)**, 3**(b) **and 4** (c) in the indicated fields at *T* = 1.8 K, 2.5 K, 5.0 K and 10 K.

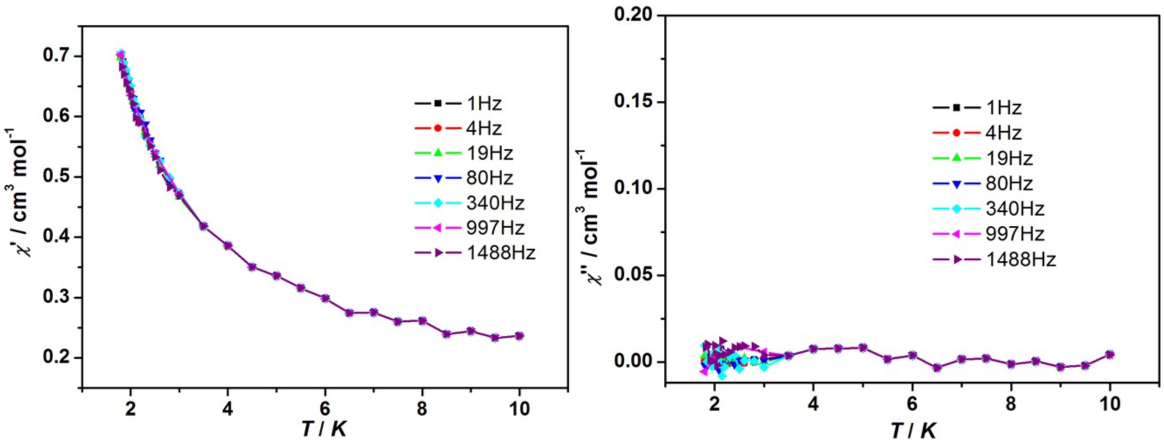

Fig

ure S6. Temperature dependence of the in-phase (χ_M') and out-of-phase (χ_M'') ac susceptibility signals in a 5 Oe ac field oscillating at 1-1488 Hz with a zero applied dc field for **1**.

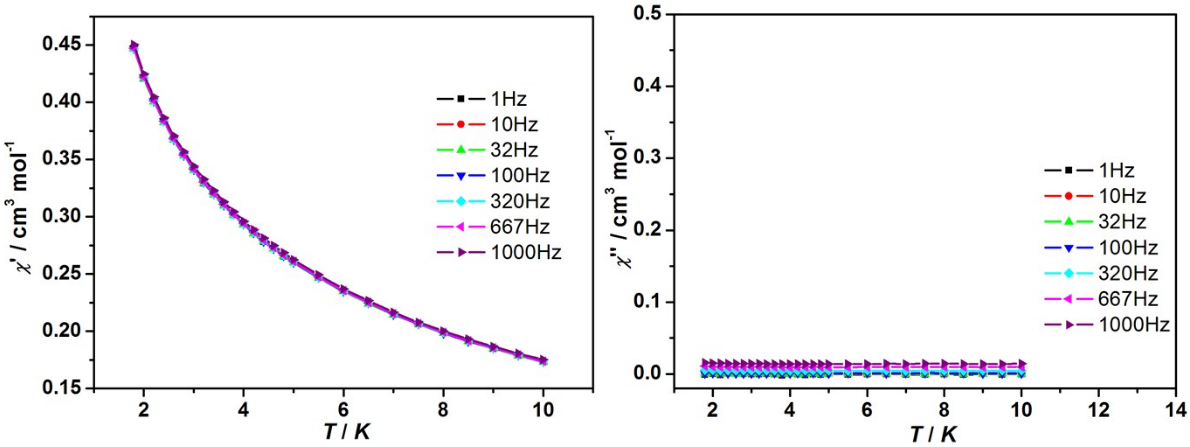

F

igure S7. Temperature dependence of the in-phase (χ_M') and out-of-phase (χ_M'') ac susceptibility signals in a 5 Oe ac field oscillating at 1-1000 Hz with a zero applied dc field for **3**.

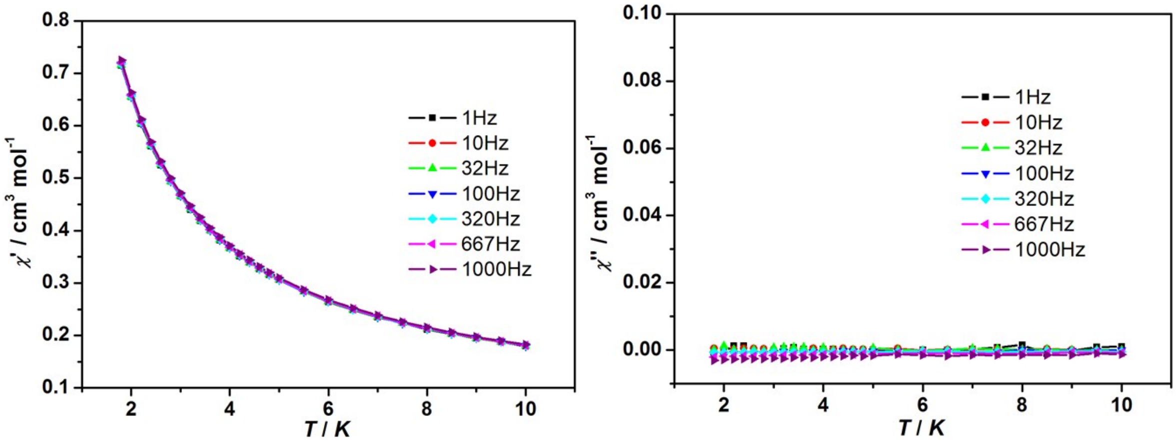

Fi

gure S8. Temperature dependence of the in-phase (χ_M') and out-of-phase (χ_M'') ac susceptibility signals in a 5 Oe ac field oscillating at 1-1000 Hz with a zero applied dc field for **4**.

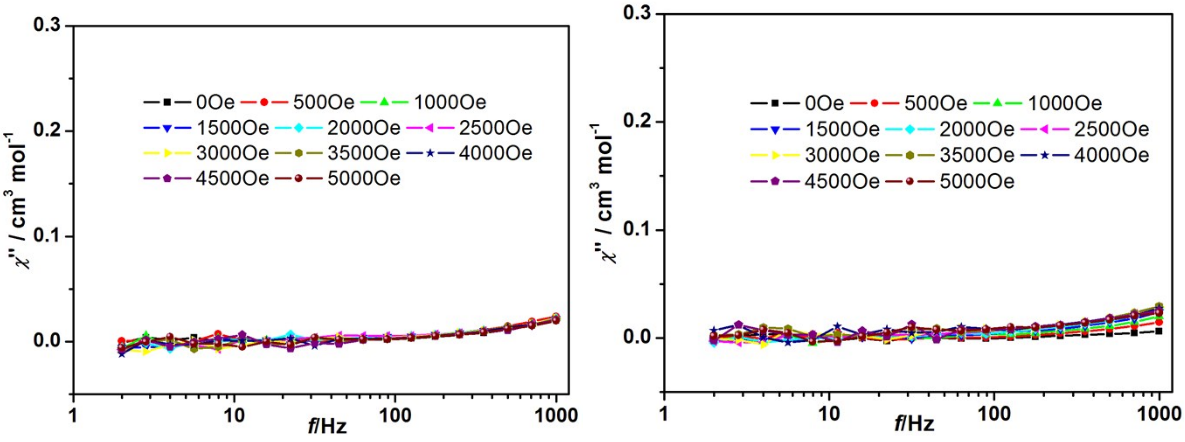

Fi

gure S9. The out-of-phase (χ_M'') signals of frequency-dependent ac susceptibility data of **3** (left) and **4** (right) under different dc fields at 2 K.

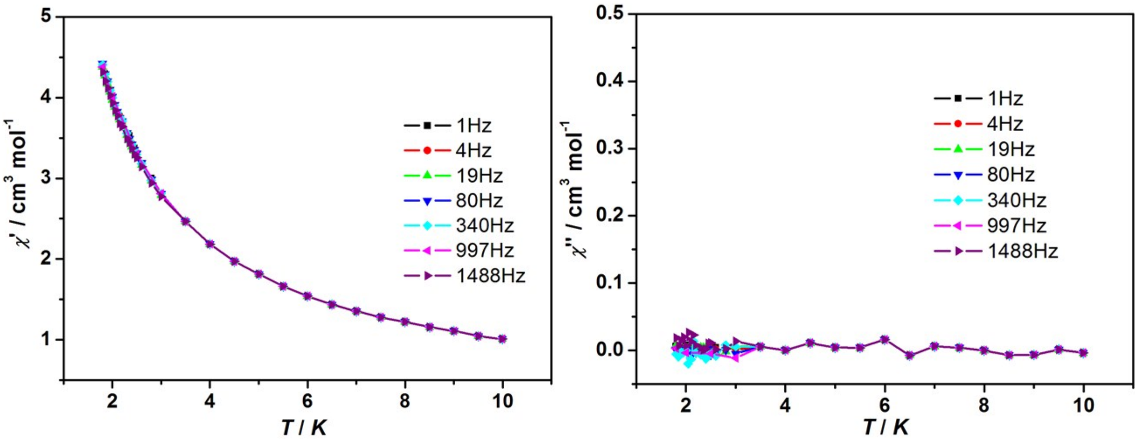

Figure S10. Temperature dependence of the in-phase (χ_M') and out-of-phase (χ_M'') ac susceptibility signals in a 5 Oe ac field oscillating at 1-1488 Hz with a zero applied dc field for **2**.

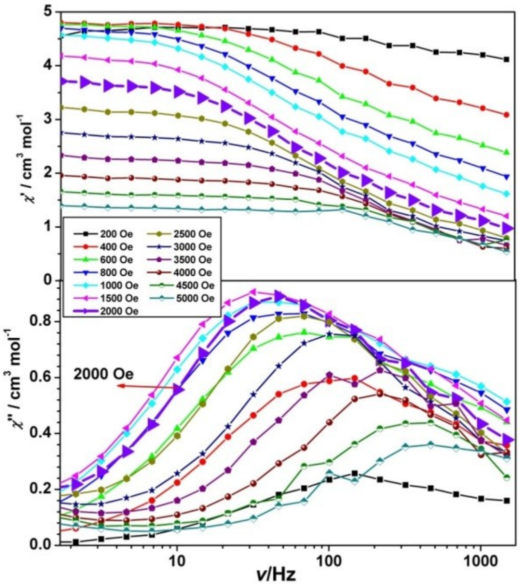

Figure S11. The in-phase (χ_M') and out-of-phase (χ_M'') signals of frequency-dependent ac susceptibility data of **2** under different dc fields at 1.8 K.

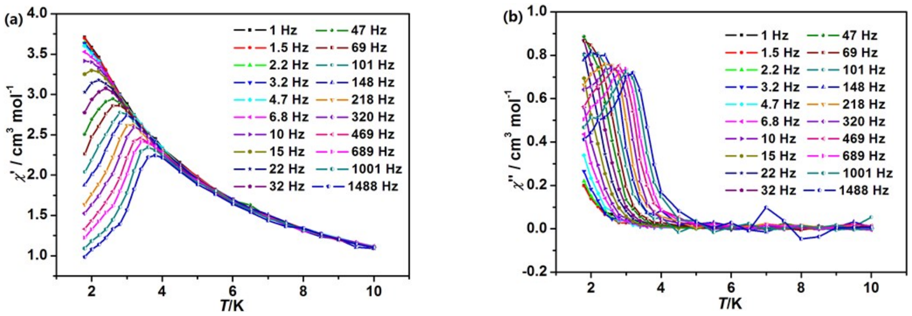

Figure S12. Temperature dependence of the in-phase χ_M' (a) and out-of-phase χ_M'' (b) in a 5 Oe ac field oscillating at 1-1488 Hz with a 2000 Oe applied dc field for **2**.

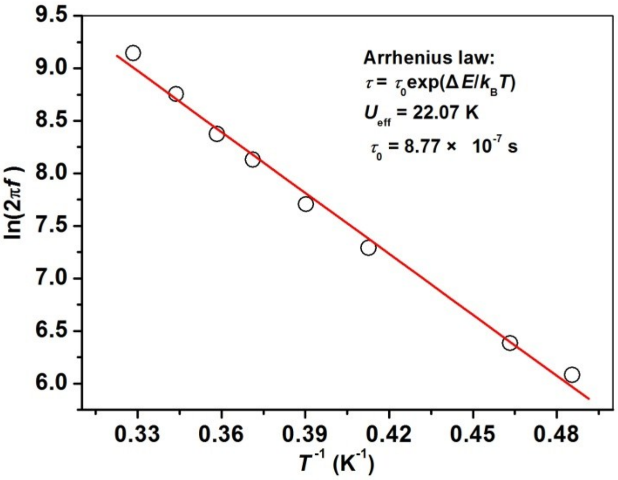

Figure S13. Plots of ln(2π*f*) versus T^{-1} of **2**, in which the frequencies (*f*) were obtained from the χ_M'' *versus T* (Figure S12). The red solid line represents the fitted results by using the equation $\tau = \tau_0\exp(U_{eff}/kT)$.

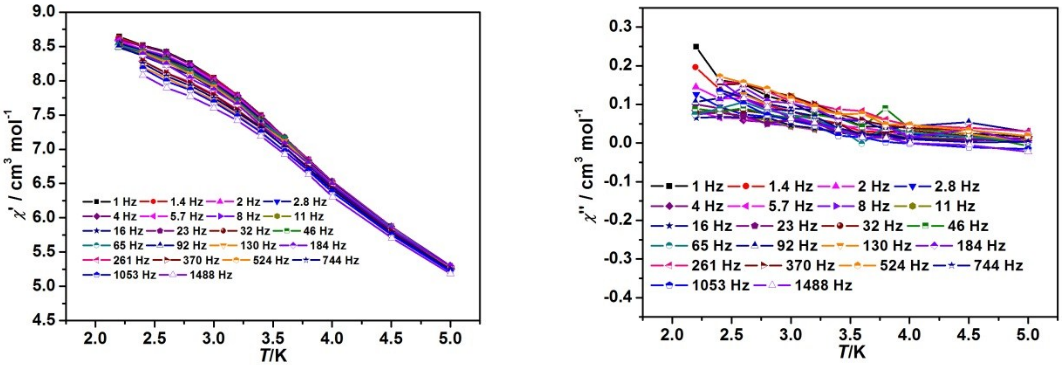

Figure S14. Temperature dependence of the in-phase χ_M' (left) and out-of-phase χ_M'' (right) in a 5 Oe ac field oscillating at 1-1488 Hz with a 2000 Oe applied dc field for the pristine sample of **2**.

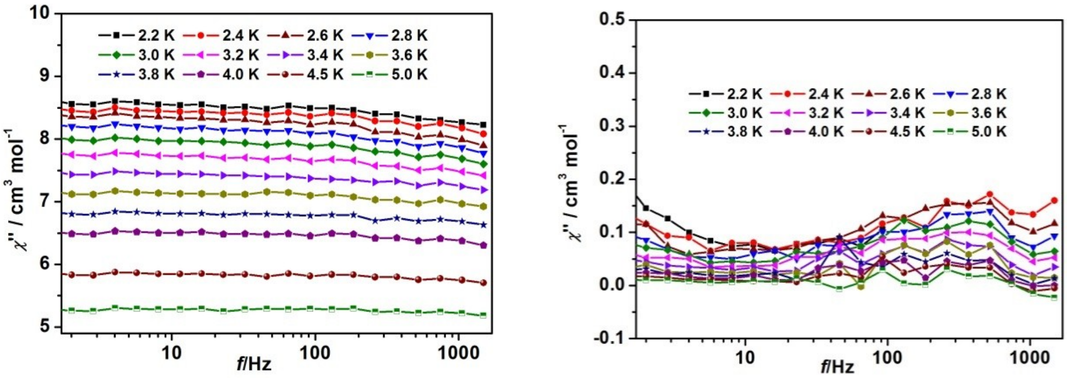

Figure S15. Frequency dependence of the in-phase χ_M' (left) and out-of-phase χ_M'' (right) in a 5 Oe ac field oscillating at 1-1488 Hz with a 2000 Oe applied dc field for the pristine sample of **2**.

Theoretical calculations

Each of complexes **1−4** have one type of individual Ln^{III} (Ln=Gd, Dy, Ho or Er) fragment and two types of individual Fe^{II} fragments, and thus we calculated one type of individual Ln^{III}(Ln=Dy, Ho or Er) fragment and two types of individual Fe^{II} fragments for each of them. Complete-active-space self-consistent field (CASSCF) calculations on individual Dy^{III}, Ho^{III}, Er^{III} or Fe^{III} fragment (see Figure S1 for calculated model structure of individual Dy^{III} fragment and two types of Fe^{II} fragments for complex **2**) extracted from the compound on the basis of single-crystal X-ray determined geometry have been carried out with MOLCAS 8.2[S1] program package. During the calculations of Ln^{III} (Ln= Dy, Ho or Er) fragment, individual Ln^{III} fragment for **2−4** was calculated keeping the experimentally determined structure of the corresponding compound while replacing the neighboring Ln^{III} ion by diamagnetic Lu^{III} and the four Fe^{III} ions by diamagnetic Zn^{II}. During the calculations of Fe1^{II} fragment for **1−4**, the influence of distance Ln^{III} (Ln= Gd, Dy, Ho or Er) ions were taken into account by the closed-shell La^{III} ab initio embedding model potentials (AIMP; La.ECP.deGraaf.0s.0s.0e-La-(LaMnO3.).[S2], and two Fe ions were taken into account by the closed-shell Zn^{II} ab initio embedding model potentials (AIMP; Zn.ECP.Lopez-Moraza.0s.0s.0e-AIMP-KZnF3.)[S2], respectively In the calculations of Fe2^{III} fragment for **1−4**, we keeping the experimentally determined structure of the corresponding compound while replacing the neighboring Ln^{III} ion by diamagnetic Lu^{III} and the influence of distance Fe^{III} were taken into account by the closed-shell Zn^{II} ab initio embedding model potentials (AIMP; Zn.ECP.Lopez-Moraza.0s.0s.0e-AIMP-KZnF3.) .

The basis sets for all atoms are atomic natural orbitals from the MOLCAS ANO-RCC library: ANO-RCC-VTZP for Dy^{III}, Ho^{III}, Er^{III} or Fe^{II} ions, respectively; VTZ for close O or N; VDZ for distant atoms. The calculations employed the second order Douglas-Kroll-Hess Hamiltonian, where scalar relativistic contractions were taken into account in the basis set and the spin-orbit couplings were handled separately in the restricted active space state interaction (RASSI-SO) procedure. For individual Ln^{III} fragment, active electrons in 7 active spaces include all *f* electrons (CAS (9 in 7 for Dy^{III}, 10 in 7 for Ho^{III}, 11 in 7 for Er^{III})) in the CASSCF calculation. To exclude all the doubts, we calculated all the roots in the active space. We have mixed the maximum number of spin-free state which was possible with our hardware (all from 21 sextets, 128 from 224 quadruplets and 130 from 490 doublets for individual Dy^{III} fragment; all from 35 septuplets, 150 from 210 triplets and 120 from 196 singlets for individual Ho^{III} fragment; all from 35 quadruplets and all from 112 doublets for individual Er^{III} fragment). For individual Fe^{III} fragment, active electrons in 5 active spaces include all *d* electrons (CAS(5 in 5)) in the CASSCF calculation. To exclude all the doubts, we calculated all the roots in the active space. We have mixed the maximum number of spin-free states which was possible with our hardware (all from 1 quintets, all from 24 triplets and all from 60 singlets). SINGLE_ANISO[S3] program was used to obtain zero-field splitting parameters D (E) (cm^{-1}), the $\boldsymbol{g}$ tensors, energy levels, magnetic axes, *et al.,* based on the above CASSCF/RASSI calculations.

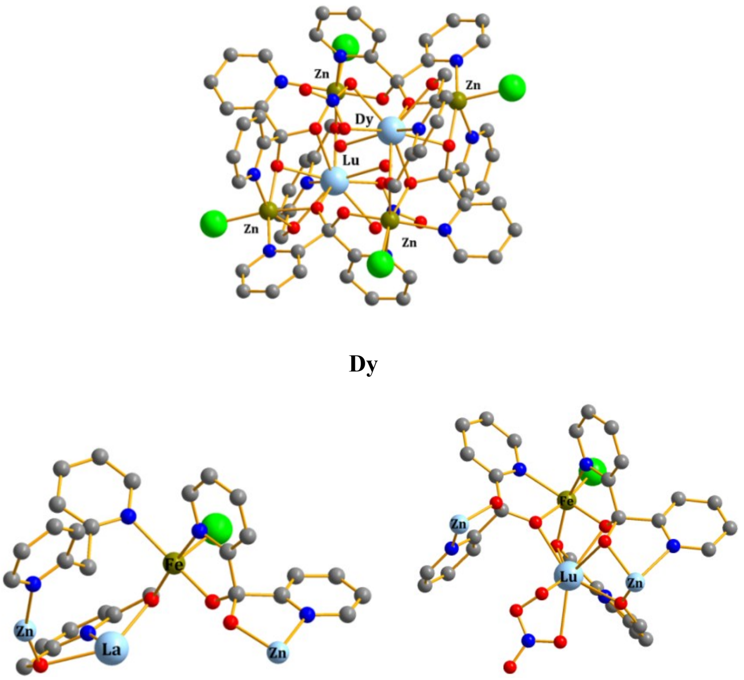

Dy

Fe1 **Fe2**

Figure S16. Calculated model structure of individual Dy^{III} or Fe^{II} fragment for complex **2**; H atoms are omitted.

Table S10. Calculated energy levels (cm^{-1}), g (g_x, g_y, g_z) tensors and m_J values of the lowest eight or nine spin-orbit states for individual Dy^{III}, Ho^{III} or Er^{III} fragments, the calculated zero-field splitting parameters D (E) (cm^{-1}) and g (g_x, g_y, g_z) tensors of the lowest spin-orbit state for individual Fe^{III} fragments using CASSCF/RASSCI with MOLCAS 8.2.

1

	Fe1	**Fe2**
CAS	(5, 5)	(5, 5)
*S*pin	$S_{Fe} = 5/2$	$S_{Fe} = 5/2$
$D(E)$	−0.09(0.02)	0.05(−0.02)
g	2.002 2.002 2.002	2.001 2.001 2.001

2

	Fe1	**Fe2**	KDs		**Dy**	
CAS	(5, 5)	(5, 5)		E/cm^{-1}	***g***	m_J
*S*pin	$S_{Fe} = 5/2$	$S_{Fe} = 5/2$	1	0.0	0.045 0.080	±15/2

					19.471	
$D(E)$	−0.08(0.02)	−0.06(−0.02)	2	84.6	0.483 1.084 14.820	±13/2
$\boldsymbol{g}$	2.002 2.002 2.002	2.002 2.002 2.002	3	120.6	0.196 0.891 16.506	±9/2
			4	176.7	3.876 4.446 11.422	±11/2
			5	236.5	1.551 4.623 8.104	±5/2
			6	270.9	2.316 4.555 14.351	±3/2
			7	332.5	0.836 1.452 15.510	±7/2
			8	466.5	0.036 0.108 19.253	±1/2

3

	Fe1	**Fe2**	KDs		**Ho**	
CAS	(5, 5)	(5, 5)		E/cm^{-1}	$\boldsymbol{g}$	m_J
Spin	$S_{\mathrm{Fe}} = 5/2$	$S_{\mathrm{Fe}} = 5/2$	1	0.0 4.2	0.000 0.000 17.220	±8
$D(E)$	−0.08(−0.03)	−0.05(0.02)	2	63.4 75.5	0.000 0.000 13.205	±7
$\boldsymbol{g}$	2.002 2.002 2.002	2.002 2.002 2.002	3	109.7 122.6	0.000 0.000 15.431	±6
			4	141.6 170.7	0.000 0.000 9.913	±4
			5	189.1 208.0	0.000 0.000 11.766	±5
			6	252.6 257.2	0.000 0.000 10.214	±3

			7	274.2		0
			8	283.0 290.4	0.000 0.000 10.784	±2
			9	343.4 344.7	0.000 0.000 17.317	±1
4						
	Fe1	**Fe2**	KDs	**Er**		
CAS	(5, 5)	(5, 5)		*E*/cm^{-1}	***g***	m_J
D(*E*)	0.08(0.03)	−0.05(0.02)	1	0.0	0.646 1.009 15.669	±15/2
g	2.002 2.002 2.002	2.002 2.002 2.002	2	64.8	3.253 3.975 9.404	±5/2
			3	82.5	2.480 3.268 10.261	±9/2
			4	150.4	2.599 4.795 9.548	±13/2
			5	188.6	0.186 3.900 9.983	±7/2
			6	219.5	2.309 4.128 11.264	±11/2
			7	291.9	0.976 1.492 11.994	±3/2
			8	382.1	0.439 1.098 15.550	±1/2

Table S11. Wave functions with definite projection of the total moment | m_J > for the lowest two spin-orbit states of individual Ln^{III} fragments (Dy^{III}, Ho^{III} and Er^{III}) for **2**−**4**.

	E/cm^{-1}	wave functions
2_Dy	0.0	95%|±15/2>
	84.6	77%|±13/2>+5%|±7/2>+6%|±5/2>

3_Ho	0.0	62%|±8>+23%|±6>+5%|±5>
	4.2	
	63.4	28%|±7>+14%|±5>+16%|±4>+15%|±2>+14%|±2>+10%|±2>
	75.5	
4_Er	0.0	64%|±15/2>+17%|±11/2>+18%|±9/2>
	64.8	4%|±15/2>+8%|±13/2>+12%|±11/2>+6%|±9/2>+11%|±7/2> +28%|±5/2>+5%|±3/2>+26%|±1/2>

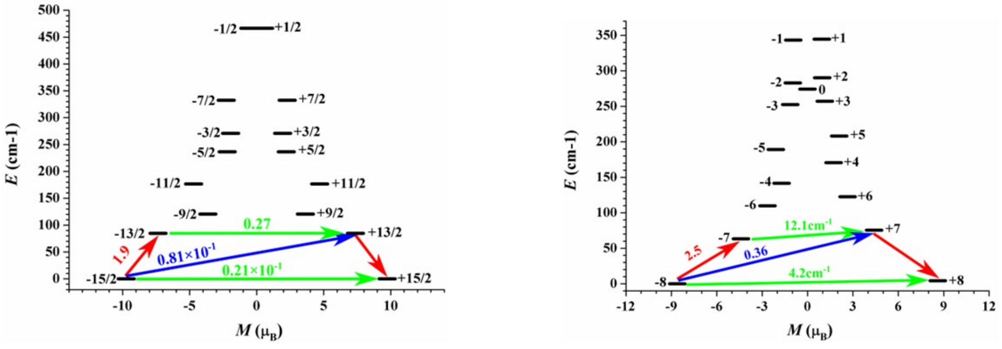

2_Dy **3_Ho**

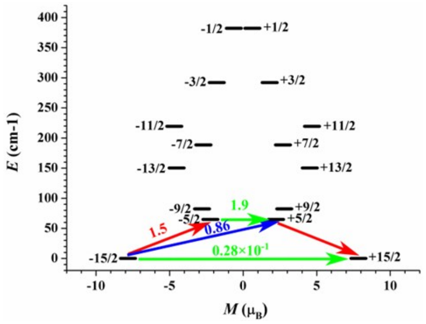

4_Er

Figure S17. Magnetization blocking barriers in individual Ln^{III} fragments (Dy^{III}, Ho^{III} and Er^{III}) of **2**–**4**. The thick black lines represent the spin-orbit states as a function of their magnetic moment along the magnetic axis. The green lines correspond to the diagonal matrix element of the transversal magnetic moment; the blue lines represent Orbach relaxation processes. The path shown by the red arrows represents the most probable path for magnetic relaxation in the corresponding compounds. The numbers at each arrow stand for the mean absolute value of the corresponding matrix element of transition magnetic moment.

To fit the total interactions in complexes **2**–**4**, we calculated individual Ln^{III} (Ln=Dy, Ho or Er) fragment using CASSCF to obtain the corresponding magnetic properties. And then, the exchange interaction between the magnetic centers is considered within the Lines model,[S4] The Lines model is effective and has been successfully used widely in the research field of *d* and *f* single-molecule magnets.[S5]

For complexes **2**–**4**, we only consider three types of *J*.

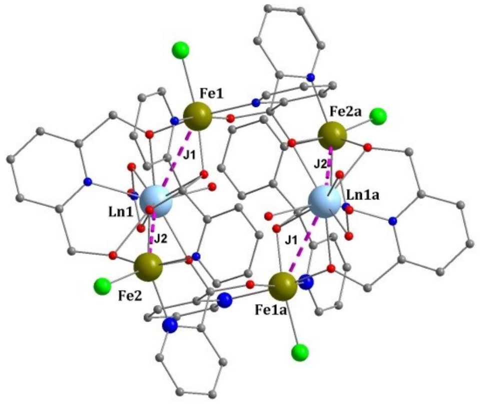

Figure S18. Two types of J_1 and J_2 in complexes **2**–**4** (Ln=Dy, Ho and Er).

The exchange Hamiltonian is:

$$\hat{H}_{exch} = -J_1(\hat{S}_{Fe1}\hat{\tilde{S}}_{Ln1} + \hat{S}_{Fe1a}\hat{\tilde{S}}_{Ln1a}) - J_2(\hat{\tilde{S}}_{Fe2}\hat{\tilde{S}}_{Ln1} + \hat{S}_{Fe2a}\hat{\tilde{S}}_{Ln1a}) \qquad (1)$$

The J_1 and J_2 are parameters of the total magnetic interactions between Fe1-Ln1 (Fe1a-Ln1a) and Fe2-Ln1 (Fe2a-Ln1a), respectively. The $\tilde{S} = \pm 1/2$ is the ground pseudospin on Ln^{III} (Dy^{III}, Ho^{III} and Er^{III}) sites. The spin $S = \pm 5/2$ is on Fe^{III} sites. The Fe^{III} ions in three complexes were considered as isotropic, and the average g value was set as 2.0 during the fitting. The total coupling constants were fitted through comparison of the computed and measured magnetic susceptibility using the Poly_ANISO program.[S3]

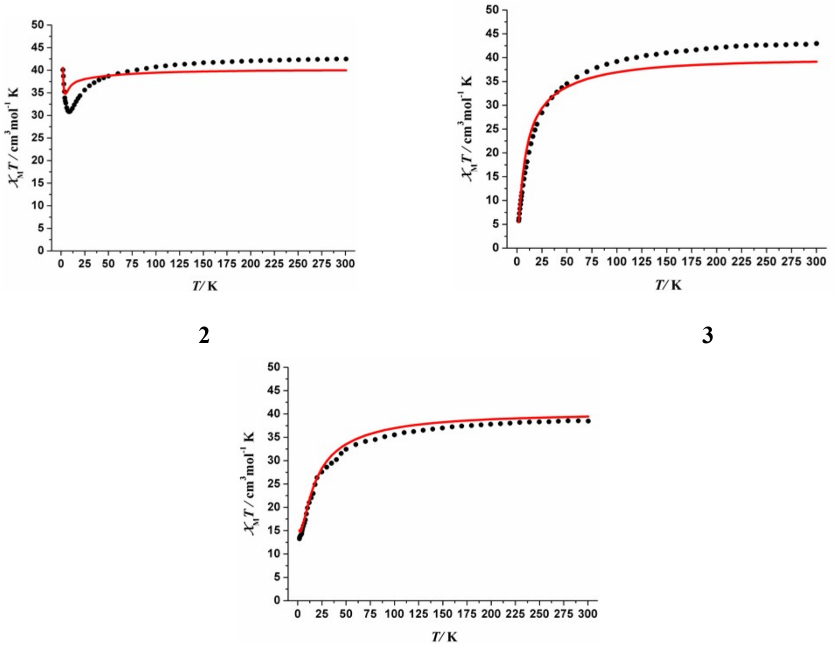

2

3

4

Figure S19. Calculated (red solid line) and experimental (circle dot) data of magnetic susceptibilities of complexes **2**−**4**. The intermolecular interactions zJ' of 2−4 were fitted to 0.04 cm^{-1}, −0.01 cm^{-1} and 0.06 cm^{-1}, respectively.

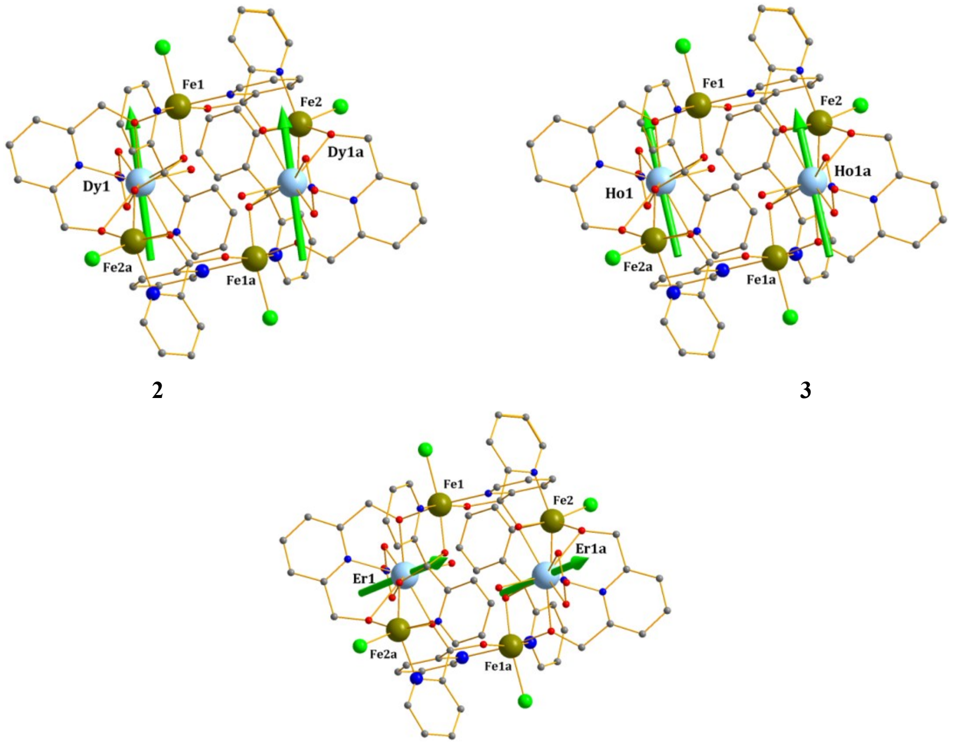

2

3

4

Figure S20. Calculated orientations of the local main magnetic axes of the ground spin-orbit state on Ln^{III} (Dy^{III}, Ho^{III} and Er^{III}) ions of complexes **2**−**4**.

References:

S1 (a) F. Aquilante, J. Autschbach, R. K. Carlson, L. F. Chibotaru, M. G. Delcey, L. De Vico, I. Fdez. Galván, N. Ferré, L. M. Frutos, L. Gagliardi, M. Garavelli, A. Giussani, C. E. Hoyer, G. Li Manni, H. Lischka, D. Ma, P. Å. Malmqvist, T. Müller, A. Nenov, M. Olivucci, T. B. Pedersen, D. Peng, F. Plasser, B. Pritchard, M. Reiher, I. Rivalta, I. Schapiro, J. Segarra‐Martí, M. Stenrup, D. G. Truhlar, L. Ungur, A. Valentini, S. Vancoillie, V. Veryazov, V. P. Vysotskiy, O. Weingart, F. Zapata, R. Lindh, MOLCAS 8: New Capabilities for Multiconfigurational Quantum Chemical Calculations across the Periodic Table, *J. Comput. Chem*., **2016**, *37*, 506.

S2 Seijo, L.; Barandiarán, Z. *Computational Chemistry: Reviews of Current Trends*; World Scientific, Inc.: Singapore, 1999; pp 455−152.

S3 (a) Chibotaru, L. F.; Ungur, L.; Soncini, A. *Angew. Chem. Int. Ed.*, **2008**, *47*, 4126. (b) Ungur, L.; Van den Heuvel, W.; Chibotaru, L. F. *New J. Chem.*, **2009**, *33*, 1224. (c) Chibotaru, L. F.; Ungur, L.; Aronica, C.; Elmoll, H.; Pilet, G.; Luneau, D. *J. Am. Chem. Soc.*, **2008**, *130*, 12445.

S4 Lines, M. E. *J. Chem. Phys*. **1971**, *55*, 2977.

S5 (a) Mondal, K. C.; Sundt, A.; Lan, Y. H.; Kostakis, G. E.; Waldmann, O.; Ungur, L.; Chibotaru, L. F.; Anson, C. E.; Powell, A. K. *Angew. Chem. Int. Ed*. **2012**, *51*, 7550. (b) Langley, S. K.; Wielechowski, D. P.; Vieru, V.; Chilton, N. F.; Moubaraki, B.; Abrahams, B. F.; Chibotaru, L. F.; Murray, K. S. *Angew. Chem. Int. Ed*. **2013**, *52*, 12014.